Ultrafast Dynamics of Hydrogen Bond Exchange in Aqueous Ionic Solutions

Sungnam Park,[†,§] Michael Odelius,[‡] and Kelly J. Gaffney*[,†]

PULSE Institute, SLAC National Accelerator Laboratory, Stanford University, Stanford, California 94305, and Fysikum, AlbaNova University Center, Stockholm University, SE-106 91 Stockholm, Sweden

Received: February 23, 2009

The structural and dynamical properties of aqueous ionic solutions influence a wide range of natural and biological processes. In these solutions, water has the opportunity to form hydrogen bonds with other water molecules and anions. Knowing the time scale with which these configurations interconvert represents a key factor to understanding the influence of molecular scale heterogeneity on chemical events in aqueous ionic solutions. We have used ultrafast IR spectroscopy and Car−Parrinello molecular dynamics (CPMD) simulations to investigate the hydrogen bond (H-bond) structural dynamics in aqueous 6 M sodium perchlorate ($NaClO_4$) solution. We have measured the H-bond exchange dynamics between spectrally distinct water−water and water−anion H-bond configurations with 2DIR spectroscopy and the orientational relaxation dynamics of water molecules in different H-bond configurations with polarization-selective IR pump−probe experiments. The experimental H-bond exchange time correlates strongly with the experimental orientational relaxation time of water molecules. This agrees with prior observations in water and aqueous halide solutions, and has been interpreted within the context of an orientational jump model for the H-bond exchange. The CPMD simulations performed on aqueous 6 M $NaClO_4$ solution clearly demonstrate that water molecules organize into two radially and angularly distinct structural subshells within the first solvation shell of the perchlorate anion, with one subshell possessing the majority of the water molecules that donate H-bonds to perchlorate anions and the other subshell possessing predominantly water molecules that donate two H-bonds to other water molecules. Due to the high ionic concentration used in the simulations, essentially all water molecules reside in the first ionic solvation shells. The CPMD simulations also demonstrate that the molecular exchange between these two structurally distinct subshells proceeds more slowly than the H-bond exchange between the two spectrally distinct H-bond configurations. We interpret this to indicate that orientational motions predominantly dictate the rate of H-bond exchange, while translational diffusion must occur to complete the molecular exchange between the two structurally distinct subshells around the perchlorate anions. The 2DIR measurements observe the H-bond exchange between the two spectrally distinct H-bond configurations, but the lifetime of the hydroxyl stretch precludes the observation of the slower molecular exchange. Our 2DIR experiments and CPMD simulations demonstrate that orientational motions predominantly equilibrate water molecules within their local solvation subshells, but the full molecular equilibration within the first solvation shell around the perchlorate anion necessitates translational motion.

I. Introduction

Aqueous ionic solutions lubricate the chemical machinery of natural and biological systems. While the unique and incompletely understood properties of water receive significant and justified attention,[1] natural and biological processes also depend critically on the ionic species present in solution.[2] While the dissolution of ions in water requires the solvation of the ions by water molecules, leading to a disruption of the hydrogen bond (H-bond) network, the extent to which dissolved ions disturb the structure of liquid water remains unresolved.[2−5] A full description of ionic solutions requires a detailed understanding of the structure and dynamics of water molecules in different H-bond configurations, the rate of H-bond exchange between these H-bond configurations, and the rate of molecular exchange within and between ionic solvation shells.

The hydroxyl stretch frequency of water provides an excellent sensor for local H-bond structure, which ultrafast infrared (IR) spectroscopy has harnessed to monitor H-bond dynamics.[3,6−14] A variety of molecular dynamics simulations[12,15,16] and time-resolved IR experiments have been performed to characterize the dynamics of water[10−13,17] and various ionic solutions.[3,9,14,16,18,19] For the study of H-bond structural dynamics, polarization-selective IR pump−probe experiments have been used to measure the orientational relaxation dynamics while two-dimensional infrared (2DIR) spectroscopy has been employed to determine the spectral diffusion dynamics. Orientational relaxation and spectral diffusion dynamics provide an effective monitor of H-bond dynamics in water and the influence of dissolved ions on these dynamics. All studies to date demonstrate that dissolved ions slow down H-bond structural dynamics in highly concentrated aqueous ionic solutions,[9,14] but the nature of this dynamical transformation has yet to be determined. Bakker and co-workers have emphasized the heterogeneity of the dynamics in aqueous ionic solutions, particularly in aqueous perchlorate (ClO_4^-) solutions by comparing the dynamics of hydroxyl groups H-bonded to ClO_4^- anions and those H-bonded

* To whom correspondence should be addressed. E-mail: kjgaffney@slac.stanford.edu.
† SLAC National Accelerator Laboratory.
‡ Stockholm University.
§ Present address: Department of Chemistry, Korea University, Seoul, 136-701, South Korea.

10.1021/jp9016739 CCC: $40.75
Published on Web 05/12/2009

to another water molecule.[3] From the orientational anisotropy measurements, they attribute the slowing of the water dynamics in aqueous ionic solutions to water molecules H-bonded to ClO_4^- and conclude that ions only weakly modify the dynamics of all other water molecules in aqueous solutions.[3] More recently, ion−water exchange dynamics have been studied with aqueous $NaBF_4$ solutions with 2DIR.[20] They observe that the exchange between water−water and water−anion H-bonds occurs more slowly than the rate of orientational relaxation. As will be discussed, we observe a stronger correlation between the H-bond exchange time and the orientational relaxation time.

Here, we have used concentrated aqueous $NaClO_4$ solutions as a model system to study the H-bond structural dynamics of water in aqueous ionic solutions. Unlike most aqueous salt solutions, aqueous $NaClO_4$ solutions have two spectrally distinct hydroxyl stretch peaks that correspond to two distinct H-bond configurations: (1) water molecules H-bonded to other water molecules and (2) those H-bonded to perchlorate ions and non-H-bonded. We have used 2DIR spectroscopy to study the H-bond exchange dynamics between these two spectrally distinct subensembles and the spectral diffusion dynamics of each subensemble. Polarization-selective IR pump−probe spectroscopy has been performed to measure the orientational relaxation and vibrational population relaxation dynamics of each subensemble. We have also performed Car−Parrinello molecular dynamics (CPMD) simulations on aqueous 6 M $NaClO_4$ solution. A comprehensive description of the H-bond structure and dynamics of aqueous $NaClO_4$ solutions emerges based on the relative time scales of the orientational relaxation, spectral diffusion, and H-bond exchange between spectrally distinct H-bond configurations, and molecular exchange between structurally distinct molecular configurations within the first solvation shell of the perchlorate anions.

The structural analysis relies predominantly on the spatial distribution function (SDF) extracted from the CPMD simulations, rather than relying solely on the radial distribution function (RDF) for structural information. The SDFs clearly show that in aqueous 6 M $NaClO_4$ solution the first solvation shell around the anions in solution consists of two radially and angularly distinct subshells. These structurally distinct subshells correspond to (1) water molecules that predominantly donate a H-bond to another water molecule and a perchlorate anion (W_{WP}) and (2) water molecules that predominantly donate two H-bonds to other water molecules (W_{WW}). The analysis of the structural dynamics shows that the H-bond exchange rate strongly correlates with the orientational relaxation rates, as seen previously in MD simulations of water and aqueous sodium chloride solutions.[17,18] These simulation results have been interpreted with an orientational jump model that attributes H-bond exchange to prompt and large angular rotations.[17,18] Comparison of the experimental and CPMD simulation results lead us to attribute the H-bond exchange predominantly to orientational relaxation of water molecules. The final stage of H-bond structural relaxation involves the molecular exchange between the two structurally distinct subshells within the first solvation shell of the perchlorate anion. This molecular exchange necessitates center-of-mass translational motion and proceeds more slowly than the orientational relaxation that leads to H-bond exchange between spectrally distinct H-bond configurations. The MD simulations indicate that this molecular exchange occurs too slowly to be observed prior to vibrational relaxation of the OD stretch.

II. Methodology

A. Ultrafast Infrared (IR) Spectroscopy. The laser system employed in the experiments was built based on a design that has been described in detail elsewhere.[21] Briefly, 800 nm pulses were generated by a Ti:Sapphire oscillator (KM Laser) and regenerative amplifier (Spitfire, Spectra-Physics) laser system at 1 kHz. The 800 nm pulses with 45 fs duration and ~0.8 mJ per pulse were used to pump an optical parametric amplifier (OPA, Spectra-Physics) to produce near-IR pulses at ~1.3 and ~2.0 μm which were utilized to generate mid-IR pulses at ~4 μm in a 0.5 mm thick $AgGaS_2$ crystal by difference frequency generation (DFG). The power spectrum of the mid-IR pulses had a Gaussian envelope with a ~270 cm^{-1} bandwidth (full width at half-maximum). After generation, the mid-IR pulses propagate through an experimental setup purged with dry and CO_2 scrubbed air. We measured the pulse chirp with frequency-resolved optical gating (FROG) measurements in a transient grating geometry.[21] We used CaF_2 plates with different thicknesses to compensate for the linear dispersion introduced by other dielectric materials in the setup, particularly a Ge Brewster plate. This setup produced transform-limited mid-IR pulses with an intensity fwhm of ~55 fs at the sample.

The experimental details and principles of two-dimensional infrared (2DIR) spectroscopy have been described in detail elsewhere.[14,21−23] Briefly, we focus three mid-IR pulses with an off-axis parabolic mirror (fl =150 cm) onto the sample in a noncollinear geometry and collimate the beams after the sample with another off-axis parabolic mirror (fl =150 cm). The spot size of the IR beams at the sample position is approximately 50 μm in diameter. We control the relative time of these three pulses with computer controlled translation stages. The sample emits the signal in a unique phase-matched direction, which we overlap with a local oscillator pulse for heterodyne detection. A grating in a spectrometer disperses the heterodyned signal onto the top stripe of a dual 32 × 2 element mercury−cadmium−telluride (MCT) array detector with high speed data acquisition electronics (Infrared Associates and Infrared Systems Development Corp.). A portion of the IR beam that does not go through the sample is sent to the bottom stripe of the array and used as a reference beam. In 2DIR experiments, there are three experimental time variables. The delay between the first and second pulses corresponds to the evolution time (τ), the delay between the second and third pulses corresponds to the waiting time (T_w), and the delay between the third pulse and the emitted signal corresponds to the detection time (t). We measure the 2DIR signal by scanning τ at fixed T_w and frequency resolving the heterodyned signal onto the pixel array detector. To construct the 2DIR spectra, we must Fourier transform the τ and the t time periods. The spectrometer performs the detection time (t) Fourier transform to generate the ω_m axis, while we numerically Fourier transform the τ time period after collecting the τ-dependent interferogram for each value of ω_m. This Fourier transformation provides the ω_τ axis. 2DIR spectra are displayed with initial frequency ω_τ and final frequency ω_m at a fixed T_w time. We generate purely absorptive 2DIR spectra with the dual scan method in which nonrephasing and rephasing 2DIR spectra are measured separately by two different input pulse sequences and added.[24]

In IR pump−probe experiments, an IR pump pulse excites a molecular system to the first vibrational excited state ($v = 1$), and subsequently the time evolution of the molecular system is measured by a time-delayed IR probe pulse. The details of the IR pump−probe experiments have been described elsewhere.[23,25] Mid-IR pulses are split into the pump and probe beams with a

relative intensity of 9:1 and are focused onto the sample. The probe beam is collimated after the sample and is dispersed through a spectrometer onto the MCT array detector. The wiregrid polarizers are placed in the pump and probe beam before the sample and in front of the spectrometer. The parallel, $S_{\parallel}(t)$, and perpendicular, $S_{\perp}(t)$, components of the pump−probe signals at each frequency are measured with the polarization of the pump beam parallel and perpendicular to the probe beam, respectively.

D_2O and $NaClO_4$ salt were purchased from Sigma-Aldrich and were used as received. An isotopically mixed water solution of 5% HOD in H_2O was prepared by mixing 2.5 wt % D_2O with H_2O. Aqueous $NaClO_4$ solution was prepared by directly dissolving $NaClO_4$ salt in the isotopically mixed water solution. This dilute isotopically mixed water solution of 5% HOD in H_2O was used for 2DIR and IR pump−probe measurements to avoid undesired vibrational excitation transfer (Förster resonant excitation transfer[26,27] of the OD stretch mode which would interfere with other dynamics of interest). For simplicity, the isotopically mixed water sample without $NaClO_4$ salt will be referred to as neat water in the remainder of the paper. The samples were housed in cells containing two CaF_2 windows (3 mm thick) and a Teflon spacer with a thickness adjusted to obtain optical density of ∼0.3 including the H_2O background absorption for all solutions studied. A range of 2340−2700 cm^{-1} was measured with a frequency resolution of ∼6 cm^{-1}. 2DIR spectra of HOD in aqueous 6 M $NaClO_4$ solution were collected at $T_w = 0.2$, 0.4, 0.6, 1.0, 1.5, 2.0, 3.0, 4.0, 5.0, 7.0, and 9.0 ps. All experiments were conducted at 22 °C.

B. Ab Initio Molecular Dynamics Simulations. Ab initio Car−Parrinello molecular dynamics (CPMD) simulations[28] were performed to characterize the structural and dynamical properties of aqueous 6 M $NaClO_4$ solution. The CPMD simulations give an accurate description of many-body effects in concentrated aqueous ionic solutions, against which classical force fields can be evaluated,[29,30] since CPMD calculates the forces on the fly with periodic density functional calculations using a gradient-corrected density functional, BLYP.[31,32] However, since the computationally taxing CPMD methodology limits the system size to 7 Na^+ and 7 ClO_4^- ions dissolved in 46 water molecules and simulation duration to 20 ps, we also performed 100 times longer duration and 8 times larger simulations with a classical force field (parameters for the ions were taken from Heinje et al.[29] and water is described by the flexible SPC force field[33]) that confirmed that the size and duration limits of the CPMD calculation do not distort the local structure and dynamics. The periodic density functional theory (DFT) calculations used pseudopotentials in combination with an 85 Ry kinetic energy cutoff for the plane wave expansion of the Kohn−Sham wave functions. For hydrogen, a local pseudopotential parametrized with one Gaussian was used. The pseudopotential for oxygen was of Troullier−Martins type[34] expressed in the Kleinman−Bylander form,[35] and were nonlocal in the $l = 0$ channel. Goedecker pseudopotentials were used for sodium and chlorine.[36,37] We model the aqueous 6 M $NaClO_4$ solution in the NVT ensemble with a 1.446 g/cm^3 density and use a 0.1 fs time-step and a fictitious electron mass of 500 au. We set the Nose−Hoover thermostat[38−40] to 350 K to compensate for the lack of a quantum treatment of the hydrogen atoms and the limitations of density functionals employed.[41,42] We initialized the 6 ps equilibration trajectory with the classical MD simulation and simulated two different deuterated systems. We used the simulation of 6 M $NaClO_4$ with 1:45=DOH:H_2O (20 ps) to study the H-bond structural and reorientational dynamics and the simulation of 6 M $NaClO_4$ with 46 DOH (9 ps) to obtain the IR spectrum to get an appreciable OD component in the total electric dipole and to validate a local mode description of the hydroxyl stretch band. For reference, we also performed simulations of pure liquid water at 1.0 g/cm^3 and 350 K with either 64 DOH (11 ps) or 64 H_2O (18 ps) molecules.

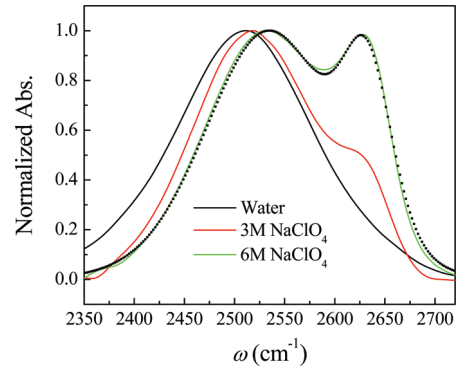

Figure 1. FTIR spectra of the OD stretch of HOD in aqueous, 3, and 6 M $NaClO_4$ solutions. The H_2O background has been subtracted. FTIR spectrum of the OD stretch of HOD in isotopically mixed water is shown for comparison. In aqueous $NaClO_4$ solutions, the lower frequency peak results from the OD_W subensemble while the higher frequency peak results from the OD_P subensemble. The dotted black line is the linear spectrum obtained from the response function calculation. See the text for more detail.

III. Results

A. FTIR Spectroscopy. Molecular dynamics simulations have shown that the hydroxyl stretch frequency depends linearly on the electric field projected along the hydroxyl bond measured at the position of the hydrogen atom.[10,43,44] This makes the frequency of the hydroxyl stretch vibration very sensitive to its H-bond configuration in both neat water and aqueous ionic solutions.[44] In general, H-bond structural changes lead to changes in the projected electric field and manifest themselves in the peak position and width of the hydroxyl stretch spectrum of water.[23] Figure 1 displays the OD stretch region of the FTIR spectra of HOD in neat water and aqueous 3 and 6 M $NaClO_4$ solutions. The OD spectrum of HOD in aqueous $NaClO_4$ solutions has two spectrally distinct OD peaks that can be accurately fit with the sum of two Gaussian peaks. As $NaClO_4$ concentration increases, the low frequency peak blue shifts and widens, while the high frequency peak blue shifts slightly and increases in amplitude. The high frequency peak is associated with water molecules in the anionic hydration shell of perchlorate ions. Water molecules in the cationic hydration shell cannot be distinguished from those in bulk water because cations interact mostly with the oxygen atom of water and have little effects on the hydroxyl stretch frequency.

As will be shown in Section III.F, molecular dynamics simulations corroborate our assignment of the two spectrally distinct hydroxyl stretch peaks in aqueous 6 M $NaClO_4$ solution. The low frequency OD peak at 2534 cm^{-1} results from water molecules that donate a H-bond to a water molecule, while the high frequency OD peak at 2633 cm^{-1} results from water molecules that donate a H-bond to an anion or do not donate a H-bond. The CPMD simulation shows that the non-H-bonded hydroxyl groups are extremely short-lived, as observed previously for isotopically mixed water.[12] As a result, it is assumed that the non-H-bonded hydroxyl groups do not contribute to the dynamics occurring on picosecond time scales. Our analysis of experimental and simulation results emphasizes the H-bond

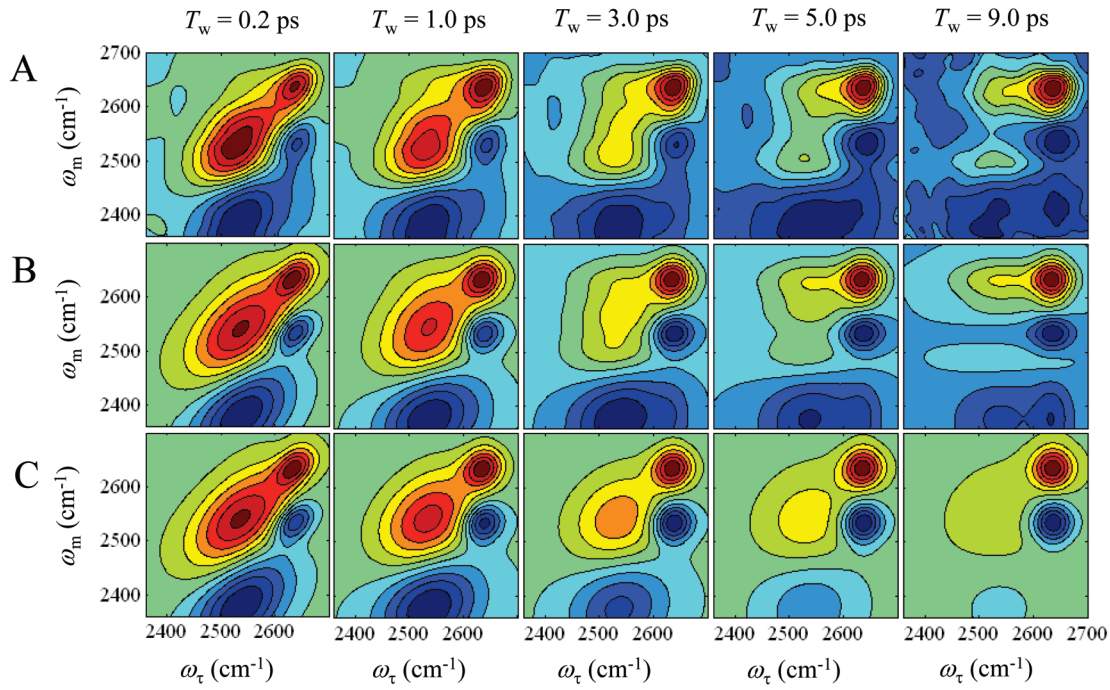

Figure 2. 2DIR spectra for a series of T_w shown with 10% contour lines. (A) Experimental spectra of the OD stretch measured from 5% HOD in H_2O with 6 M $NaClO_4$. The high frequency peak at $\omega_\tau = \omega_m = 2633$ cm^{-1} corresponds to the OD_P configuration with an anharmonicity of 100 cm^{-1}. The low frequency peak at $\omega_\tau = \omega_m = 2534$ cm^{-1} corresponds to OD_W configuration with an anharmonicity of 153 cm^{-1}. (B) Calculated spectra with a response function formalism that includes a two-species exchange kinetics. (C) Calculated spectra without H-bond exchange ($k_{P-W} = k_{W-P} = 0$). Clearly, H-bond exchange must be included to accurately reproduce the experimental spectra.

structural dynamics occurring on picosecond time scales and thus we focus mainly on the H-bond dynamics of the stable water-perchlorate (OD_P) and the water−water (OD_W) H-bond configurations. This will be discussed in greater detail in Sections III.E and III.F.

B. 2DIR Spectroscopy. The hydroxyl stretch spectrum in aqueous $NaClO_4$ solution consists of two spectrally distinct H-bond configurations that thermally interconvert on the picosecond time scale. This fact makes aqueous $NaClO_4$ solutions an ideal model system for 2DIR studies of H-bond exchange dynamics. 2DIR spectroscopy monitors thermal equilibrium dynamics occurring on the picosecond time scale[45−48] by vibrationally labeling molecules with their initial hydroxyl (OD) stretch frequencies and then correlating these initial frequencies (ω_τ) with the final frequencies (ω_m) of the molecules after an experimentally controlled waiting time (T_w). Thus, 2DIR spectroscopy can determine when an initially frequency-labeled OD_W hydroxyl stretch switches to an OD_P hydroxyl stretch after a given T_w.

Figure 2A displays 2DIR spectra at a series of T_w times measured on HOD in aqueous 6 M $NaClO_4$ solution. The positive peaks shown in red along the diagonal ($\omega_\tau = \omega_m$) result from the fundamental vibrational transition ($v = 0 \rightarrow 1$). The negative peaks appearing in blue below the diagonal arise from the $v = 1 \rightarrow 2$ transition with the value of ω_m red shifted relative to ω_τ by the vibrational anharmonicity. The T_w-dependent 2DIR spectra reflect a variety of dynamical processes. Vibrational population decay and orientational relaxation result in T_w-dependent peak amplitudes, spectral diffusion results in T_w-dependent peak shapes, and population exchange between subensembles results in T_w-dependent cross peak amplitudes.

In the 2DIR spectra shown in Figure 2A, the narrow diagonal peak at $\omega_\tau = \omega_m = 2633$ cm^{-1} results from OD_P while the broad diagonal peak at $\omega_\tau = \omega_m = 2534$ cm^{-1} results from OD_W. As will be shown below, the vibrational lifetime of OD_W is approximately 2 times shorter than that of OD_P. As a result, the broad diagonal peak at $\omega_\tau = \omega_m = 2534$ cm^{-1} decays faster as T_w increases. The peak shape is diagonally elongated at short T_w times and becomes symmetrical as T_w increases. This is a signature of spectral diffusion, which will be discussed later in detail. A cross peak at $\omega_\tau = 2534$ cm^{-1} and $\omega_m = 2633$ cm^{-1} gradually increases in amplitude with increasing T_w. The T_w-dependent cross peak amplitude in the 2DIR spectra provides the spectroscopic signature for H-bond exchange between the OD_P and OD_W configurations. By monitoring the T_w-dependent rise of this cross peak amplitude, the exchange rate between OD_P and OD_W can be determined. The cross peak at $\omega_\tau = 2534$ cm^{-1} and $\omega_m = 2633$ results from OD_W switching to OD_P. Since this exchange occurs at equilibrium, the exchange process from OD_P to OD_W will also generate a cross peak at $\omega_\tau = 2633$ cm^{-1} and $\omega_m = 2534$ cm^{-1} with an equal probability. Experimentally, the $v = 1 \rightarrow 2$ transition of OD_P is negative and obscures this cross peak. Switching from OD_P to OD_W however does result in a cross peak between the $v = 1 \rightarrow 2$ transitions at $\omega_\tau = 2633$ cm^{-1} and $\omega_m = 2370$ cm^{-1} as clearly seen in the 2DIR spectrum at $T_w = 9.0$ ps in Figure 2A.

C. IR Pump−Probe Spectroscopy. The orientational and vibrational population relaxation dynamics can be determined by performing polarization-selective IR pump−probe spectroscopy on the OD stretch of HOD in 6 M $NaClO_4$ solution. As mentioned in the previous section, in aqueous 6 M $NaClO_4$ the $v = 0 \rightarrow 1$ transition (2533 cm^{-1}) of the OD stretch in OD_W is significantly overlapped with the $v = 1 \rightarrow 2$ transition of the OD stretch in OD_P. Thus, we measured the pump−probe signals at probe frequencies of 2630 cm^{-1} for OD_P and 2371 cm^{-1} for OD_W. Pump−probe signals of the hydroxyl stretch of HOD in aqueous solutions relax to a constant offset in several picoseconds. This offset results from the deposition of heat in the sample following vibrational population relaxation. When the excited state molecules relax to the ground state, their vibrational

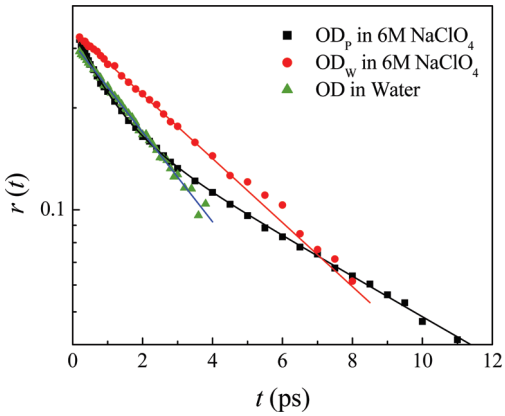

Figure 3. Orientational anisotropy decay, $r(t)$. $r(t)$ for OD_P subensemble (black square) was measured at $\omega_m = 2630$ cm^{-1} ($v = 0 \rightarrow 1$ transition). The $v = 1 \rightarrow 2$ transition of the OD stretch in the OD_P subensemble is overlapped with the $v = 0 \rightarrow 1$ transition of the OD stretch in OD_W subensemble. $r(t)$ for OD_W (red circle) subensemble was measured at $\omega_m = 2371$ cm^{-1} ($v = 1 \rightarrow 2$ transition). $r(t)$ for isotopically mixed water was measured with the $v = 1 \rightarrow 2$ transition at $\omega_m = 2388$ cm^{-1} (green triangle). The exponential fits to $r(t)$ are shown with solid lines.

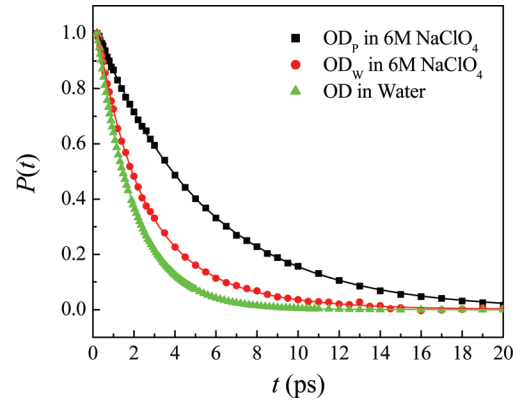

Figure 4. Vibrational population decays of the OD of HOD in two subensembles in aqueous 6 M $NaClO_4$ solution. Vibrational population decay for OD_W subensemble was measured at the $v = 1 \rightarrow 2$ transition (2371 cm^{-1}). Vibrational population decay of the OD of HOD in isotopically mixed water measured at 2509 cm^{-1} ($v = 0 \rightarrow 1$ transition) is shown for comparison.

TABLE 1: Orientational Relaxation Parameters

	center freq (cm^{-1})	a_1	τ_{or1} (ps)	a_2	τ_{or2} (ps)
6 M $NaClO_4$	2630 (OD_P)	0.15 ± 0.01	1.0 ± 0.3	0.19 ± 0.01	7.3 ± 0.5
	2371 (OD_W)			0.34 ± 0.01	5.0 ± 0.5
water	2510			0.35 ± 0.01	2.6 ± 0.2
	2388			0.31 ± 0.02	3.3 ± 0.5

TABLE 2: Population Relaxation Parameters

	center freq (cm^{-1})	A	T_{1S} (ps)	$1 - A$	T_{1L} (ps)
6 M $NaClO_4$	2630 (OD_P)	1	5.2 ± 0.1		
	2371 (OD_W)	0.61 ± 0.01	1.8 ± 0.1	0.39	3.9 ±0.1
water	2509	1	1.8 ± 0.1		
	2388	1	1.8 ± 0.1		

energy dissipates into the bath leading to rapid local heating of the sample. In IR pump−probe experiments, the transient OD spectrum gets blue shifted gradually as the vibrational population relaxation proceeds. Similarly, FTIR absorption spectra of the hydroxyl stretch of water blue shift with increasing temperature. We subtract this heating contribution from the pump−probe signals to get accurate orientational anisotropy and population decay dynamics.[49−51] It should be noted that the heating contribution in the pump−probe signal gets smaller as the salt concentration increases.

We measure the pump−probe signal with the probe beam polarization parallel, $S_{||}(t)$, and perpendicular, $S_{\perp}(t)$, to the pump beam polarization. The orientational anisotropy, $r(t)$, equals

$$r(t) = \frac{S_{||}(t) - S_{\perp}(t)}{S_{||}(t) + 2S_{\perp}(t)} = \frac{2}{5}C_{or}(t) \qquad (1)$$

where $C_{or}(t)$ is the second-order Legendre polynomial of the transition dipole correlation function, $\langle P_2[\boldsymbol{\mu}(t)\cdot\boldsymbol{\mu}(0)]\rangle$. The vibrational population decay, $P(t)$, equals

$$P(t) = S_{||}(t) + 2S_{\perp}(t) \qquad (2)$$

Figures 3 and 4 display the orientational anisotropy, $r(t)$, and the vibrational population decay, $P(t)$, measured at 2630 cm^{-1} for OD_P and 2371 cm^{-1} for OD_W in aqueous 6 M $NaClO_4$ solution. The orientational anisotropy decays has been fit to a biexponential

$$r(t) = a_1 \exp(-t/\tau_{or1}) + a_2 \exp(-t/\tau_{or2}) \qquad (3)$$

where $\tau_{or2} > \tau_{or1}$. Table 1 lists the fit results. When compared with neat water, OD_P and OD_W have significantly slower anisotropy decay reflecting the effect of the dissolved $NaClO_4$ salt. The normalized vibrational population decays have been fit to a biexponential

$$P(t) = A \exp(-t/T_{1S}) + (1 - A)\exp(-t/T_{1L}) \qquad (4)$$

where $T_{1L} \geq T_{1S}$. Table 2 lists the fit results. The vibrational population of neat water at 2509 cm^{-1} decays monoexponentially with a lifetime of 1.8 ps. The vibrational population decay of OD_W and OD_P in aqueous 6 M $NaClO_4$ solution occur more slowly than that of the OD stretch of HOD in water measured at 2509 cm^{-1}.[52]

D. Numerical Calculation of 2DIR Spectra. The linear IR spectrum and T_w-dependent 2DIR spectra can be numerically calculated by using the response function formalism with input parameters based on diagrammatic perturbation theory. Conversely, all parameters in the response function formalism can be determined from the linear and nonlinear experimental results.[53] Kwak et al. have described the response function formalism with two-species chemical exchange and the numerical calculation of 2DIR spectra in great detail,[54] which we briefly outline here to facilitate the presentation of our results.

T_w-dependent 2DIR spectra with the interconversion between OD_P and OD_W subensembles can be calculated using the following scheme

$$\overset{T_1^P,\tau_{or}^P,C_{FFCF}^P}{\underset{\text{evolve}}{\leftarrow}} \quad OD_P \underset{k_{W-P}}{\overset{k_{P-W}}{\rightleftarrows}} OD_W \quad \overset{T_1^W,\tau_{or}^W,C_{FFCF}^W}{\underset{\text{evolve}}{\rightarrow}}$$

where k_{P-W} and k_{W-P} are the forward and backward exchange rate constants, T_1^W and T_1^P are the vibrational lifetimes, τ_{or}^W and τ_{or}^P are the orientational relaxation times, and C_{FFCF}^W and C_{FFCF}^P are the frequency-frequency correlation functions (FFCFs) of OD_W and OD_P subensembles, respectively. The equilibrium constant is given by

$$K_{eq} = \frac{[OD_W]_{eq}}{[OD_P]_{eq}} = \frac{k_{P-W}}{k_{W-P}} \qquad (5)$$

where $[OD_W]_{eq}$ and $[OD_P]_{eq}$ are the equilibrium concentrations.

Taking only the interconversion between two subensembles into account, the rate equations can be written by

$$\frac{d[OD_P]}{dt} = -k_{P-W}[OD_P] + k_{W-P}[OD_W]$$
$$\frac{d[OD_W]}{dt} = k_{P-W}[OD_P] - k_{W-P}[OD_W] \quad (6)$$

These rate equations can be analytically solved with the boundary condition, $[OD_P] + [OD_W] =$ constant, and the peak intensities in T_w-dependent 2DIR spectra are directly associated with the concentrations that are determined by the two-species exchange kinetics[55]

$$[OD]_{PP}(T_w) = [OD_P]_{eq}\frac{k_{W-P} + k_{P-W}\exp(-k_{ex}T_w)}{k_{ex}}$$
$$[OD]_{WW}(T_w) = [OD_W]_{eq}\frac{k_{P-W} + k_{W-P}\exp(-k_{ex}T_w)}{k_{ex}}$$
$$[OD]_{PW}(T_w) = [OD_P]_{eq}\frac{k_{P-W}(1 - \exp(-k_{ex}T_w))}{k_{ex}}$$
$$[OD]_{WP}(T_w) = [OD_W]_{eq}\frac{k_{W-P}(1 - \exp(-k_{ex}T_w))}{k_{ex}} \quad (7)$$

where $k_{ex} = k_{P-W} + k_{W-P}$ is the exchange rate constant, $[OD]_{PP}(T_w)$ and $[OD]_{WW}(T_w)$ are the concentrations of the diagonal peaks, and $[OD]_{PW}(T_w)$ and $[OD]_{WP}(T_w)$ are the concentrations of the cross peaks. The integrated intensity of the cross peaks in T_w-dependent 2DIR spectra depend on the exchange rate constant, $k_{ex} = k_{P-W} + k_{W-P}$.

The numerical calculation includes all of the dynamical features that are observed in the 2DIR spectra. As T_w increases, the amplitudes of peaks decay due to both vibrational population relaxation and orientational relaxation while the peak shapes change from diagonally elongated to symmetrical as a result of spectral diffusion that is quantified by the FFCF. In addition, the interconversion causes the cross peaks to grow in with increasing T_w. As mentioned in Section III.A, the OD spectrum of HOD in aqueous 6 M $NaClO_4$ solution is reasonably well described by a sum of two Gaussian functions. Accordingly, we calculate the linear and third-order nonlinear response functions for OD_P and OD_W in aqueous 6 M $NaClO_4$ solution by assuming that the fluctuations of OD_P and OD_W follow Gaussian statistics (second-order cumulant approximation) and that the transition dipole moment of the OD stretch does not depend on the frequency (Condon approximation). While prior studies have demonstrated the limitations of these approximations with respect to the hydroxyl stretch of pure water, a more sophisticated theoretical treatment resides outside the scope of this paper.[56,57] The harmonic approximation is used to scale the transition dipole moments, $\mu_{01}/\mu_{12} = \sqrt{2}$. In addition, the finite pulse duration needs to be considered for the calculation because the fwhm of the OD stretch spectrum is comparable to the bandwidth of the input IR pulses and thus the IR pulses are no longer in the impulsive limit. The finite pulse duration and the pulse interaction orders within the finite pulse duration must also be addressed when the pulses are temporally overlapped.[58] Here, the pulses used in the calculations have an intensity fwhm of 55 fs, as determined experimentally.

The vibrational lifetimes (T_1) and orientational relaxation times (τ_{or}) for OD_P and OD_W subensembles have been directly determined by polarization-selective IR pump−probe experiments and used as input parameters for the response function calculations. We discuss the limitations in used pump-probe derived population and orientational relaxation times in section IV.A. We use two Kubo terms to model the FFCFs for both the OD_P and OD_W configurations, $C_{FFCF} = \Delta_1^2 \exp(-t/\tau_1) + \Delta_2^2 \exp(-t/\tau_2)$. The second Kubo term generates an inhomogeneously broadened line width that obscures the motionally narrowed first Kubo term in the calculated linear absorption spectrum (the dotted line) shown in Figure 1. We used the center line slope (CLS) method to determine the second Kubo term time constants (τ_2) for the OD_P and OD_W subensembles.[14,23,59] We iteratively fit all other parameters in the response function formalism by minimizing the difference between the numerically calculated linear IR absorption spectrum and T_w-dependent 2DIR spectra and the experimental results. The iterative fit varied the ratios of transition dipole moments ($\mu_{01,W}/\mu_{01,P}$), the equilibrium concentrations (C_W/C_P), the H-bond exchange rate ($k_{W-P}C_W = k_{P-W}C_P$), and the Δ_1, Δ_2, and τ_1 parameters in the FFCF. Figure 2B and Figure 1 display the 2DIR spectra and the linear IR absorption spectrum of the OD stretch of HOD in aqueous 6 M $NaClO_4$ solution, respectively, calculated from the response function formalism with the best fit parameters summarized in Table 3. Most significantly, we extract H-bond forward and backward exchange rate constants, $(k_{P-W})^{-1} = 9 \pm 2$ ps and $(k_{W-P})^{-1} = 17 \pm 4$ ps, as well as a total exchange rate of $\tau_{ex} = (k_{P-W} + k_{W-P})^{-1} = 6 \pm 2$ ps. The calculated 2DIR spectra without H-bond exchange ($k_{P-W} = k_{W-P} = 0$) appear in Figure 2C for comparison. Clearly, the cross peak intensity observed experimentally in the 2DIR spectra requires H-bond exchange between the OD_P and OD_W subensembles.

E. CPMD Simulations of the Structure of Aqueous 6 M $NaClO_4$ Solution. We use a standard geometric H-bond criterion to analyze the H-bond structure: $R_{OO} < 3.5$ Å, $R_{HO} < 2.5$ Å, and $\theta_{HOO} < 30°$. Using this criterion, water molecules in aqueous 6 M $NaClO_4$ solution donate an average of 1.6 H-bonds. The simulations indicate that the solution consists of predominantly two different water species: (1) water molecules that donate two H-bonds to other water molecules (W_{WW}, 34%) and (2) water molecules that donate one H-bond to a water molecule and the other H-bond to a ClO_4^- ion (W_{WP}, 27%). In addition, a large fraction of transient water species donate only a single H-bond to either a water molecule (W_{WN}, 21%) or a ClO_4^- ion (W_{NP}, 9%). While short-lived, these species show up in the instantaneous sampling of the structure of aqueous 6 M $NaClO_4$ solution.

Radial distribution functions (RDFs), $g(r)$, and spatial distribution functions (SDFs) extracted from the CPMD simulations for the 6 M $NaClO_4$ solution appear in Figures 5 and 6. The results from classical MD simulations also appear in Figure 5A and show a reasonable structural similarity between the two simulations. Because of the high ionic concentration, the $g(r =$

TABLE 3: Parameters Used for Numerical Calculation of Linear IR Spectrum and T_w-Dependent 2DIR Spectra[a]

	T_1(ps)	τ_{or} (ps)	Δ_1 (cm^{-1})	τ_1 (ps)	Δ_2 (cm^{-1})	τ_2 (ps)	μ_{01}	conc
OD_W	2.54	5.0	57.3	0.17	37.4	3.50	1.36	1.98
OD_P	5.24	4.6	27.6	0.36	9.21	4.24	1	1

[a] The numerical calculation use single exponential decays for the population and the orientational relaxation. The values listed for T_1 and τ_{or} correspond to the best fits of the experimental data to single exponential decays.

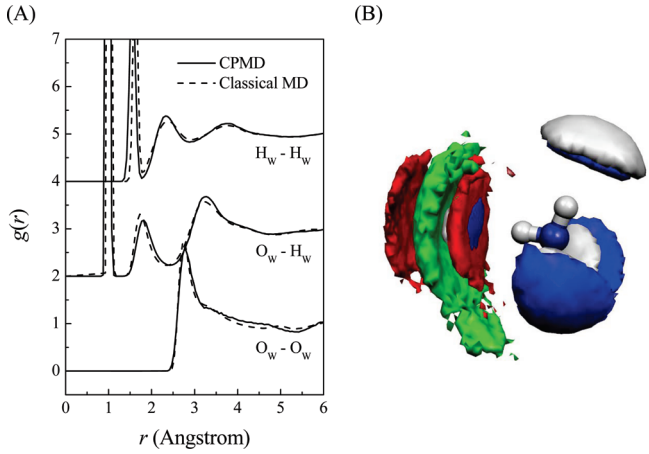

Figure 5. Radial distribution functions (RDFs) and spatial distribution function (SDF) in aqueous 6 M $NaClO_4$ solution. (A) The simulated RDF, restricted to atoms in water. (B) The SDF surrounding the water molecules in solution. The SDF is graphically displayed with the Molekel software.[67] Perchlorate (ClO_4^-): oxygen (red) and chlorine (green). Water: oxygen (blue) and hydrogen (gray).

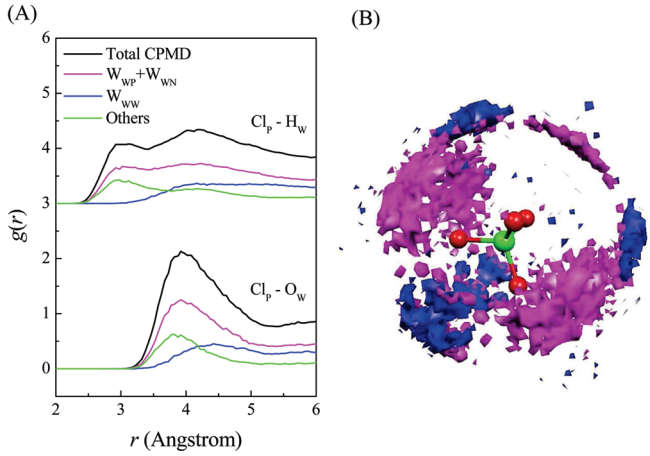

Figure 6. Radial distribution functions (RDFs) and spatial distribution function (SDF) in aqueous 6 M $NaClO_4$ solution. (A) The Cl−O_W and Cl−H_W RDF. (B) The SDF of the oxygen atoms of water molecules oriented about the ClO_4^- anion. The SDF is graphically displayed with the Molekel software.[67] The distribution in purple corresponds to oxygen atoms from W_{WP} and W_{WN} water molecules. The distribution in blue corresponds to oxygen atoms from W_{WW} water molecules.

$O_W - O_W$) in Figure 5A does not show a well-defined minimum between the first and second solvation shells, but the SDF in Figure 5B clearly shows that the roughly tetrahedral ordering observed in water persists in concentrated $NaClO_4$ solution. In order to present the average symmetry around the water molecule, we orient the coordinate system of the water molecules so that the closest oxygen atom of the ClO_4^- ion to the H-bond donor occurs around the left-most OH group. As a consequence, the distribution of other water molecules predominantly appears around the right-most OH group, although water molecules that donate two H-bonds to other water molecules also generate a significant density of water along the left OH group. Since the oxygen atom of water is not H-bonded perfectly along the Cl−O bond, there is a broad spatial distribution of Cl atoms.

Figure 6 displays RDF and SDF of different water configurations oriented about the ClO_4^- anion in solution. As shown in Figure 6A, the peak in the $g(r = Cl_P - O_W)$ for W_{WW} water molecules occurs at a larger radius than for W_{WP} water molecules. This occurs because the first solvation shell of the

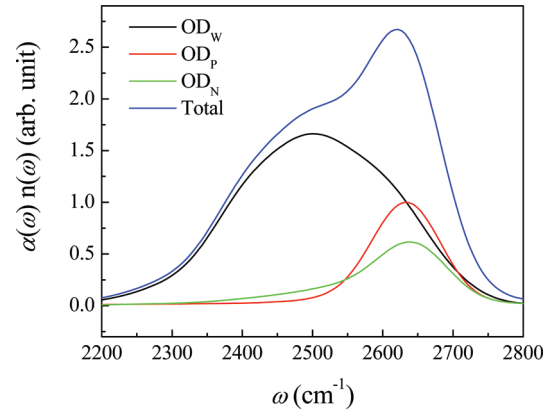

Figure 7. Linear IR spectra of the OD stretch of HOD in different H-bond configurations extracted from the CPMD simulation of aqueous 6 M $NaClO_4$ solution. The low-frequency broad peak results from the OD groups that donate a H-bonded to other water molecules (OD_W). The high frequency narrow peak results from the non-H-bonded OD groups and the OD groups that donate a H-bonded to a perchlorate anion (OD_P). The qualitative agreement between the FTIR spectrum of the OD stretch of HOD in aqueous 6 M $NaClO_4$ solution shown in Figure 1 and the CPMD simulation results strongly support the spectroscopic assignments used in our analysis of the experimental data.

ClO_4− anion is divided into two structurally distinct subshells, which we denote $W^{(1)}_{WW}$ and $W^{(1)}_{WP}$. The SDF shown in Figure 6B clearly shows that the first solvation shell around the perchlorate anion contains two radially and angularly distinct subshells, with one subshell dominated by water molecules that donate two H-bonds to other water molecules ($W^{(1)}_{WW}$) and the other subshell being dominated by water molecules that donate one H-bond to a water molecule and one to an anion ($W^{(1)}_{WP}$). As shown in Figure 6B, the O_W of $W^{(1)}_{WP}$ water molecules peak parallel to the O−Cl−O angle bisector, while the maxima in the O_W density of $W^{(1)}_{WW}$ water molecules has a tetrahedral structure, with the peaks occurring antiparallel to the Cl−O bonds on the opposite side of the ClO_4^- ion.

F. CPMD Simulations of the Linear IR Spectrum. We calculate the IR spectra by Fourier transforming the total electric dipole time correlation function, $\mathbf{M}(t)$[60−63]

$$\alpha(\omega)\cdot n(\omega) = \frac{4\pi\omega \tanh(\beta\hbar\omega/2)}{3\hbar cV}\int_{-\infty}^{\infty} dt e^{-i\omega t}\langle \mathbf{M}(t)\cdot\mathbf{M}(0)\rangle \quad (8)$$

where V is the volume, T is the temperature, $\beta = 1/kT$, $n(\omega)$ is the refractive index, and c is the speed of light in vacuum.

To assign the two OD peaks of HOD in aqueous 6 M $NaClO_4$ solution, we partition the CPMD simulation result into 1 ps time intervals and the OD spectra of HOD in different H-bond configurations are calculated in each time interval. Figure 7 displays the OD stretch spectra of HOD in different H-bond configurations. We have scaled the frequency axis so that the simulated gas phase vibrational frequency matches the experimental value. When compared with the OD stretch peaks in the experimental IR spectrum in Figure 1, the peaks in the simulated IR spectrum are broader and the relative intensity of the high and low frequency OD peaks is different. While the CPMD simulation does not quantitatively reproduce the experimental FTIR spectrum, it clearly corroborates the assignment of the OD peak at 2534 cm^{-1} to OD_W subensemble and the OD peak at 2633 cm^{-1} to OD_P subensemble. The high frequency narrow peak results from the OD groups that do not donate a H-bond (OD_N) or donate a H-bonded to a ClO_4^- ion (OD_P),

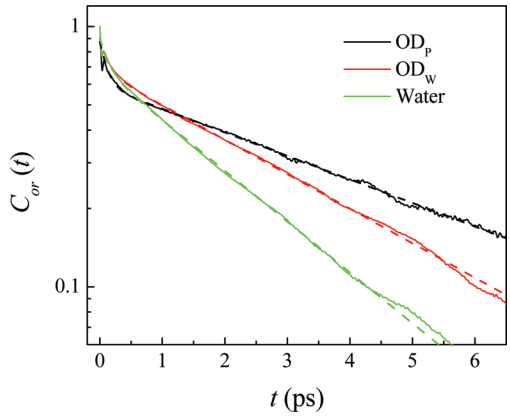

Figure 8. Orientational correlation functions, $C_{or}(t) = \langle P_2[\boldsymbol{\mu}(t)\cdot\boldsymbol{\mu}(0)]\rangle$, for OD_P (black line) and OD_W (red line) subensembles in aqueous 6 M $NaClO_4$ solution as well as isotopically mixed water (green) obtained from the CPMD simulations. The dashed lines are biexponential fits to$C_{or}(t)$.

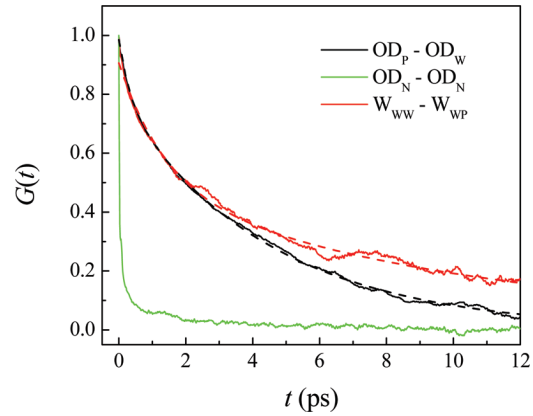

Figure 9. The H-bond exchange time cross correlation function, $G^{TCCF}(t)$, between OD_P and OD_W (black line), the H-bond lifetime autocorrelation function, $G^{TACF}(t)$, of non-H-bonded OD groups (green line), and between W_{WW} and W_{WP} (red line) obtained from the CPMD simulations. The dashed lines are biexponential fits to $G(t)$.

while the low frequency broad peak results from OD groups that donate a H-bond to another water molecule (OD_W). It turns out that both OD_N and OD_P subensembles contribute to the OD peak at the high frequency in the IR spectrum. However, as will be shown in Section III.G, the OD_N subensemble is short-lived and does not contribute to the H-bond structural dynamics occurring on picosecond time scales observed in the CPMD simulations or ultrafast IR experiments.

G. CPMD Simulations of Hydrogen Bond and Orientational Dynamics in Aqueous 6 M $NaClO_4$ Solution. We use the second-order Legendre polynomial of the transition dipole orientational time correlation function (TCF), $C_{or}(t) = \langle P_2[\boldsymbol{\mu}(t)\cdot\boldsymbol{\mu}(0)]\rangle$, to calculate the orientational anisotropy for the OD_W and OD_P subensembles. The 2 ns long classical simulations provide sufficient statistics to confirm that the orientational relaxation of the OD group in HOD does not differ from the orientational relaxation of OH groups. In the calculation of the orientational time correlation functions for OD_W and OD_P, we restrict the sampling to cases in which the OD group has retained or recovered the same H-bond configuration. We divide the resulting TCF by the appropriate H-bond lifetime time autocorrelation function (TACF) to generate the correct orientational TCF. Furthermore, for the calculation of orientational dynamics we reduce the influence of fast H-bond dynamics by neglecting H-bond fluctuations occurring faster than a picosecond. The second-order orientational correlation functions, $C_{or}(t)$, appear in Figure 8.

We calculate time correlation functions for both spectrally distinct hydroxyl stretch configurations (OD_W and OD_P) and structurally distinct molecular configurations (W_{WW} and W_{WP}). The H-bond exchange dynamics between OD_W and OD_P can be extracted by calculating the time cross correlation function (TCCF)[17,18]

$$G_{P-W}^{TCCF}(t) = 1 - \frac{\langle n_P(0)n_W(t)\rangle}{\langle n_P\rangle\langle n_W\rangle} \qquad (10)$$

where n_P is 1 when OD is H-bonded to ClO_4^- ions or not H-bonded and 0 otherwise, and n_W is 1 when OD is H-bonded to other water molecules and 0 otherwise. Here, $G_{P-W}^{TCCF}(t)$ represents the H-bond exchange dynamics between OD_P and OD_W subensembles. The fluctuation−dissipation theorem predicts $G_{P-W}^{TCCF}(t) \cong \exp(-k_{ex}t)$ with $k_{ex} = k_{P-W} + k_{W-P}$.[64] Here, the simulated H-bond exchange time, $\tau_{ex} = (k_{ex})^{-1}$, corresponds to the slow exponential decay component of $G_{P-W}^{TCCF}(t)$. In addition, the H-bond lifetime correlation function of each individual species can be obtained by calculating the TACF. For example, the H-bond lifetime TACF of OD_W subensemble equals

$$G_W^{TACF}(t) = \frac{\langle n_W(0)n_W(t)\rangle - \langle n_W\rangle^2}{\langle n_W^2\rangle - \langle n_W\rangle^2} \qquad (11)$$

This TACF represents the configurational memory of a water molecule that initially resides in the OD_W configuration before switching to the OD_P configuration.

We plot three TCFs in Figure 9. Clearly, the H-bond lifetime correlation function of the non-H-bonded hydroxyl groups in 6 M $NaClO_4$ solution decays extremely fast. This concurs with the short-lived non-H-bonded species observed in MD simulations of isotopically mixed water.[12] Consequently, the inclusion or exclusion of the non-H-bonded species has no impact on the slower relaxation dynamics observed in the simulations. Here, we need to emphasize two types of exchanges; (1) H-bond exchange between OD_W and OD_P configurations and (2) molecular exchange between W_{WW} and W_{WP} configurations. The TCCF between OD_W and OD_P configurations exhibits the time scale for the H-bond exchange between the spectrally distinct H-bond configurations which results predominantly from orientational relaxation. The decay of the slowest component of the TCCF between W_{WW} and W_{WP} molecular configurations emphasizes the time scale for exchange of water molecules between the structurally distinct subshells, which requires center-of-mass translational motion. The RDF and SDF displayed in Figure 6 clearly show the distinct radial and angular distribution of these two molecular configurations (W_{WW} and W_{WP}). In aqueous 6 M $NaClO_4$ solution, nearly all water molecules reside in the first solvation shell of the perchlorate anion. So the final exchange between these structurally distinct configurations leads to the full equilibration of the solution structure.

A critical point regarding the analysis of the chemical exchange dynamics based on these correlation functions must be understood, before proceeding to the Discussion. The W_{WP} and OD_P configurations correspond to predominantly the same molecules since both configurations reside almost exclusively in the $W_{WP}^{(1)}$ first solvation subshell around the perchlorate anion. This is distinct from the OD_W configuration, which has contributions from W_{WP} and W_{WW} water molecules. Full equilibration of the aqueous $NaClO_4$ solution requires not only

the H-bond exchange between the spectrally distinct OD_W and OD_P configurations within the first anionic solvation shell, but also the molecular exchange between the structurally distinct W_{WP} and W_{WW} configurations.

IV. Discussion

We have investigated the orientational relaxation, spectral diffusion, and H-bond exchange dynamics in aqueous 6 M $NaClO_4$ solution with ultrafast IR spectroscopy and ab initio molecular dynamics simulations. The studies have been performed to characterize the influence of dissolved ions on H-bond structural dynamics in aqueous ionic solution. Concentrated aqueous perchlorate solution represents an excellent model system for examining the influence of ions on H-bond structural dynamics in water because the hydroxyl stretch spectrum of water in aqueous 6 M $NaClO_4$ solutions is separated into two spectrally distinct peaks with the lower frequency peak corresponding to hydroxyl groups that donate a H-bond to another water molecule and the higher frequency peak corresponding to hydroxyl groups that do not donate a H-bond or donate a H-bond to a perchlorate anion. This provides the opportunity to experimentally measure the orientational relaxation and spectral diffusion dynamics of these individual subensembles independently with ultrafast IR spectroscopy, as well as the exchange dynamics between them.

A. Orientational Dynamics. As indicated in Figure 3, the orientational anisotropy of both OD_W and OD_P subensembles of water in aqueous 6 M $NaClO_4$ solution decays more slowly than that of water molecules in isotopically mixed water. In aqueous 6 M $NaClO_4$ solution, the orientational anisotropy decay of OD_P subensemble occurs more slowly than that of OD_W subensemble The slow component of the orientational anisotropy for the OD_P subensemble decays with a time constant of 7.3 $\pm$ 0.6 ps. This agrees with the 7.6 ps time constant measured by Bakker and co-workers.[3] We attribute the fast component of the orientational relaxation to the non-H-bonded OD groups that absorbs at 2633 cm^{-1}. However, for the OD_W subensemble, we get a time constant of 5.0 $\pm$ 0.5 ps, significantly slower than the 3.2 ps value reported by Bakker and co-workers. This represents an important distinction between our experiment and that of Bakker and co-workers, since we do not observe the same orientational relaxation times for OD_W subensemble, as we do for isotopically mixed water.

For isotopically mixed water, we probed the orientational anisotropy decay at 2509 cm^{-1} ($v = 0 \rightarrow 1$) and 2388 cm^{-1} ($v = 1 \rightarrow 2$). The orientational relaxation time measured at 2388 cm^{-1} exceeds the orientational relaxation time measured at 2509 cm^{-1} by a factor of $\sim$1.3, which is in agreement with previously reported results from Bakker and co-workers in isotopically mixed water.[3] Our results, however, differ significantly from those of Bakker and co-workers for the orientational anisotropy decay of OD_W subensemble in aqueous 6 M $NaClO_4$ solution as mentioned above.[3] While Bakker and co-workers observed that the orientational anisotropy decay of both OD_W and OH_W subensembles in aqueous $NaClO_4$ and $Mg(ClO_4)_2$ solutions is indistinguishable from that of isotopically mixed water, we measure the orientational anisotropy decay of the OD_W subensemble to be significantly slower than that of isotopically mixed water.

The orientational anisotropy decay obtained from the IR pump−probe experiments agrees with the trends in the orientational correlation functions, $C_{or}(t)$, extracted from MD simulations as shown in Figure 8. The $C_{or}(t)$ for the OD_P subensemble decays biexponentially with a slow exponential time constant of 4.4 $\pm$ 0.5 ps, the $C_{or}(t)$ for the OD_W subensemble decays nearly monoexponentially with a time constant of 3.2 $\pm$ 0.4 ps, and the $C_{or}(t)$ for neat water decays with a time constant of 2.2 $\pm$ 0.3 ps. While the simulated orientational relaxation decays faster than the experimental orientational relaxation, the ratios of the slowest orientational relaxation time constants ($\tau_{or}^{exp}/\tau_{or}^{sim} = 1.7 \pm 0.3$ for OD_P and $\tau_{or}^{exp}/\tau_{or}^{sim} = 1.6 \pm 0.3$ for OD_W) obtained from the CPMD simulation and polarization-selective IR pump−probe experiments agree within experimental error. The significant difference in the orientational correlation function of neat water and the OD_W subensemble extracted from the CPMD simulations supports our conclusion that the ions in concentrated aqueous $NaClO_4$ solution change the average dynamics of all water molecules, independent of their H-bond configuration.

The origin of the discrepancy between our experimental results and those previously reported by Bakker and co-workers has yet to be definitively determined. The poorly resolved nature of the two peaks in the absorption spectrum and the different experimental designs limits the value of a direct comparison between the experimental findings. Bakker and co-workers used a two-color mid-IR pump−probe setup, while we utilizes a identical pump and probe pulse and achieved spectral resolution with a spectrometer. For either implementation, separating the contributions of the two configurations proves difficult because of the non-negligible spectral overlap and may account for the different experimental observations.

Independent of the spectral overlap between the OD_P and the OP_W configurations, polarization-selective pump−probe does not measure the orientational relaxation of pure H-bond configurations. The pump−probe signal at a given ω_m frequency equals the ω_τ-integrated signal measured at the same ω_m in the 2DIR spectra. In the pump−probe configuration, the cross peak observed in the 2DIR spectra, contributes to the pump−probe signal, meaning that the observed pump−probe signal results from all molecules that possess the same frequency at the time of probe absorption, independent of their prior history (their initial frequencies). The orientational anisotropy measured at a probe frequency for the OD_P (OD_W) configuration will reflect the orientational memory of (1) molecules that started in the OD_P (OD_W) configuration and remained, as well as (2) molecules that started in the OD_W (OD_P) configuration and exchanged to the OD_P (OD_W) configuration. Since the orientational anisotropy measures both contributions simultaneously at a given probe frequency, the orientational relaxation of each contribution cannot be separated in pump−probe spectroscopy. In principle, the modeling of the 2DIR spectra can address this issue at least in part but in practice such an analysis proves difficult to perform robustly.

The mixing of H-bond configurations in the experimental pump−probe data also limits the comparison to simulation results, since the simulated orientational relaxation only includes hydroxyl groups that reside in the same H-bond configuration at time t as they possessed initially. Despite this complication, we believe it reasonable to assume that the cross peak contribution to the OD_W signal will not have a slower orientational decay than the OD_W molecules that did not exchange H-bond configurations. If this proves true, the conclusion that concentrated ionic solutions change the dynamics of water molecules even if they do not donate a H-bond to a perchlorate anion should also prove robust.

B. Spectral Diffusion Dynamics. We utilize T_w-dependent 2DIR spectra to extract the spectral diffusion dynamics of the OD_P and OD_W subensembles. Under thermal equilibrium

conditions, the H-bond structure in aqueous ionic solutions evolves by changing the H-bond lengths and angles as well as switching H-bond partners resulting in the evolution of the OD stretch frequency. The OD stretch frequency evolution within each subensemble causes the peak shape to change, while the exchange between spectrally distinct OD_W and OD_P subensembles as well as between structurally distinct W_{WW} and W_{WP} molecular configurations will lead to growth in the cross peak intensity. We monitored these spectral diffusion dynamics by inspecting the T_w-dependence of the OD_P and OD_W peak shapes residing along the diagonal in the 2DIR spectrum. The widths of these peaks projected onto the diagonal axis reflect the inhomogeneous distribution of the OD stretch frequencies within each H-bond configuration. The inhomogeneity in the OD stretch frequency leads to initial and final frequencies which remain strongly correlated for small values of T_w and generate diagonally elongated peaks, as shown in Figure 2. As the waiting time increases, spectral diffusion leads to the loss of frequency memory, which results in symmetric contours in the 2DIR spectrum. In the response function formalism, these spectral diffusion dynamics result from decay of the frequency−frequency correlation function (FFCF), $C(t) = \langle \delta\omega(0)\delta\omega(t)\rangle$. By utilizing the diagonal peaks in the 2DIR spectra to measure the spectral diffusion dynamics, we can ensure that the observed dynamics do not contain the contribution from the cross peaks present in the orientational anisotropy. This represents a clear advantage of 2DIR measurements of spectral diffusion over time-resolved hole burning[7] or homodyne photon echo techniques.[65] Table 3 lists the slowest decay component of the FFCF for OD_W water (3.5 ± 0.5 ps), OD_P water (4.2 ± 0.6 ps), and neat water ($\sim$1.5 ps).[11,66] We emphasize the slow decay because it will not be influenced by the dynamics of non-H-bonded configurations.

C. H-bond Exchange Dynamics. The dynamics of water molecules within a given H-bond configuration can be accessed by measuring the orientational and spectral diffusion dynamics, but such dynamics cannot provide a complete description of the H-bond structural dynamics of aqueous ionic solutions. A thorough description of the H-bond structural dynamics requires understanding the mechanism and time scale for the interconversion between distinct molecular and H-bond configurations.

Here, we determined the H-bond exchange time between spectrally distinct OD_P and OD_W subensembles as well as the molecular exchange between structurally distinct W_{WW} and W_{WP} configurations in aqueous 6 M $NaClO_4$ solution by using 2DIR spectroscopy and CPMD simulations. The H-bond exchange between OD_P and OD_W subensembles occurs with a time constant of 6 ± 2 ps, very similar to the orientational relaxation time constants of the OD_P and OD_W subensembles measured in polarization-selective IR pump−probe experiments. The same correlation between the H-bond exchange and orientational relaxation times has been seen in MD simulations of water and aqueous chloride solutions and described by a jump diffusion model for the H-bond exchange.[17,18] We also extract the H-bond and molecular time cross correlation functions from the CPMD simulations, as shown in Figure 9. The H-bond TCCF between spectrally distinct OD_P and OD_W subensembles has been fit to a biexponential function with a slow time constant of 4.4 ± 0.5 ps, while the molecular TCCF between structurally distinct W_{WW} and W_{WP} subensembles has been fit to a biexponential with a slow time constant of 10 ± 2 ps. The slow component of the H-bond TCCF between OD_P and OD_W subensembles emphasizes the H-bond exchange predominantly within the $W_{WP}^{(1)}$ solvation subshell around the perchlorate ions and occurs on a similar time scale as the orientational anisotropy decay of the OD_P subensemble. We get a ratio between the measured and simulated H-bond exchange times, $\tau_{HB}^{exp}/\tau_{HB}^{sim} = 1.4 \pm 0.5$, similar to that observed for the orientational relaxation times. The consistently faster dynamics observed in the CPMD simulations may result from the 350 K temperature used in the simulation. The use of an elevated temperature represents a common method designed to compensate for the classical treatment of the proton motion in the simulation.[41] While this precludes the direct quantitative comparison of experiment to simulation, the comparison of trends remains valuable. The slow component of the molecular TCCF between W_{WW} and W_{WP} subensembles emphasizes the exchange of water molecules between the first solvation subshells $W_{WP}^{(1)}$ and $W_{WW}^{(1)}$.

Experimentally, the off-diagonal cross peak intensities will contain all of the dynamics that lead to the full equilibration in aqueous 6 M $NaClO_4$ solution and complete loss of configurational memory. The simulation results indicate that we should see biexponential exchange dynamics. We have looked for biexponential exchange dynamics in the response function calculations of the experimental data, but the vibrational lifetime of the OD stretch does not allow the observation of the molecular exchange between the first solvation subshells around the perchlorate anion.

V. Concluding Remarks

We have investigated H-bond structural dynamics in aqueous 6 M $NaClO_4$ with ultrafast IR spectroscopy and Car−Parrinello molecular dynamics simulations. The aqueous $NaClO_4$ solution has two spectrally distinct hydroxyl stretch peaks. The lower frequency peak corresponds to hydroxyl groups that donate a H-bond to another water molecule, while the higher frequency peak corresponds to hydroxyl groups that do not donate a H-bond or donate a H-bond to a perchlorate ion. This spectroscopic distinction between hydroxyl groups in different H-bond configurations allows us to measure the orientational and spectral dynamics of each H-bond configuration independently, as well as the time scale for interconversion between these configurations. The dynamics extracted from ultrafast IR experiments and CPMD simulations have allowed us to construct a detailed account of the H-bond structural dynamics in this solution.

The orientational anisotropy decay and H-bond exchange dynamics extracted from ultrafast IR experiments and CPMD simulations occur with similar time constants. Such behavior has been seen in MD simulations of neat water and aqueous chloride solution and been attributed to large orientational jumps that lead to both H-bond exchange and orientational anisotropy decay.[18] The observation of a similar correlation in the orientational anisotropy decay and H-bond exchange dynamics in both ultrafast IR experiments and CPMD simulations suggests that the same orientational jump model may apply to the aqueous $NaClO_4$ solution. Conclusive assignment of the orientational and H-bond dynamics to orientational jumps awaits further detailed analysis of the CPMD simulation results.

The radial and spatial distribution functions extracted from the CPMD simulations also present a clear picture of radial and angular segregation of water molecules that donate two H-bonds to other molecules (W_{WW}) and water molecules that donate one H-bond to a water molecule and one to a perchlorate anion (W_{WP}). The CPMD simulations show that the molecular exchange between structurally distinct W_{WW} and W_{WP} configurations proceeds more slowly than the H-bond exchange between the spectrally distinct OD_W and OD_P configurations because it requires center-of-mass translation of water molecules.

Our complementary use of ultrafast IR spectroscopy and CPMD has provided a detailed qualitative description of the

structure and dynamics of aqueous 6 M $NaClO_4$. H-bond exchange occurs predominantly through orientational motions within structurally distinct solvation subshells around the perchlorate anion. The full structural relaxation requires molecular exchange between these two structurally distinct solvation subshells. This involves center-of-mass translation of water molecules and proceeds roughly two times slower than the H-bond exchange that occurs within a given subshell. This persistent structural heterogeneity clearly distinguishes aqueous ionic solutions from pure water and could influence fast dynamical events in aqueous ionic solutions, such as photochemical transformations.

Acknowledgment. S.P. and K.J.G. thank the U.S. Department of Energy and the W. M. Keck Foundation for financial support, M. D. Fayer for the illuminating discussion of 2DIR spectroscopy and water dynamics, K. Kwak for initial 2DIR calculation source code, and J. Sung for experimental assistance. M.O. thanks the Swedish Research Council (VR) for support and gratefully acknowledges generous grants of computer time at the Swedish National Supercomputer Center (NSC) and Center for Parallel Computing (PDC).

References and Notes

(1) Ball, P. *Nature* **2008**, *452*, 291.
(2) Ball, P. *Chem. Rev.* **2008**, *108*, 74–108.
(3) Omta, A. W.; Kropman, M. F.; Woutersen, S.; Bakker, H. J. *Science* **2003**, *301*, 347–349.
(4) Krekeler, C.; Site, L. D. *J. Phys.: Condens. Matter* **2007**, *19*, 192101.
(5) Mancinelli, R.; Botti, A.; Bruni, F.; Ricci, M. A.; Soper, A. K. *Phys. Chem. Chem. Phys.* **2007**, *9*, 2959–2967.
(6) Graener, H.; Ye, T. Q.; Laubereau, A. *J. Chem. Phys.* **1989**, *90*, 3413–16.
(7) Laenen, R.; Rausch, C.; Laubereau, A. *Phys. Rev. Lett.* **1998**, *80*, 2622–2625.
(8) Bratos, S.; Gale, G. M.; Gallot, G.; Hache, F.; Lascoux, N.; Leicknam, J. C. *Phys. Rev. E* **2000**, *61*, 5211.
(9) Kropman, M. F.; Bakker, H. J. *Science* **2001**, *291*, 2118–2120.
(10) Fecko, C. J.; Eaves, J. D.; Loparo, J. J.; Tokmakoff, A.; Geissler, P. L. *Science* **2003**, *301*, 1698–1702.
(11) Asbury, J. B.; Steinel, T.; Stromberg, C.; Corcelli, S. A.; Lawrence, C. P.; Skinner, J. L.; Fayer, M. D. *J. Phys. Chem. A* **2004**, *108*, 1107–1119.
(12) Eaves, J. D.; Loparo, J. J.; Fecko, C. J.; Roberts, S. T.; Tokmakoff, A.; Geissler, P. L. *Proc. Natl. Acad. Sci. U.S.A.* **2005**, *102*, 13019–13022.
(13) Cowan, M. L.; Bruner, B. D.; Huse, N.; Dwyer, J. R.; Chugh, B.; Nibbering, E. T. J.; Elsaesser, T.; Miller, R. J. D. *Nature* **2005**, *434*, 199.
(14) Park, S.; Fayer, M. D. *Proc. Nat. Acad. Sci. U.S.A.* **2007**, *104*, 16731–16738.
(15) Rey, R.; Moller, K. B.; Hynes, J. T. *J. Phys. Chem. A* **2002**, *106*, 11993–11996.
(16) Lawrence, C. P.; Skinner, J. L. *J. Chem. Phys.* **2003**, *118*, 264–272.
(17) Laage, D.; Hynes, J. T. *Science* **2006**, *311*, 832–835.
(18) Laage, D.; Hynes, J. T. *Proc. Nat. Acad. Sci. U.S.A.* **2007**, *104*, 11167–11172.
(19) Laage, D.; Hynes, J. T. *J. Phys. Chem. B* **2008**, *112*, 7697–7701.
(20) Moilanen, D. E.; Wong, D.; Rosenfeld, D. E.; Fenn, E. E.; Fayer, M. D. *Proc. Natl. Acad. Sci. U.S.A.* **2009**, *106*, 375–380.
(21) Park, S.; Kwak, K.; Fayer, M. D. *Laser Phys. Lett.* **2007**, *4*, 704–718.
(22) Zheng, J.; Kwak, K.; Fayer, M. D. *Acc. Chem. Res.* **2007**, *40*, 75–83.
(23) Park, S.; Moilanen, D. E.; Fayer, M. D. *J. Phys. Chem. B.* **2008**, *102*, 5279–5290.
(24) Khalil, M.; Demirdoven, N.; Tokmakoff, A. *Phys. Rev. Lett.* **2003**, *90* (4), 04740.
(25) Moilanen, D. E.; Piletic, I. R.; Fayer, M. D. *J. Phys. Chem. C* **2007**, *111*, 8884–8891.
(26) Woutersen, S.; Bakker, H. J. *Nature* **1999**, *402*, 507–509.
(27) Gaffney, K. J.; Piletic, I. R.; Fayer, M. D. *J. Chem. Phys.* **2003**, *118*, 2270–2278.
(28) Car, R.; Parrinello, M. *Phys. Rev. Lett.* **1985**, *55*, 2471.
(29) Heinje, G.; Luck, W. A. P.; Heinzinger, K. *J. Phys. Chem. A.* **1987**, *91*, 331–338.
(30) Krienke, H.; Opalka, D. *J. Phys. Chem. C* **2007**, *111*, 15935–15941.
(31) Becke, A. D. *Phys. Rev. A* **1988**, *38*, 3098–3100.
(32) Lee, C.; Yang, W.; Parr, R. G. *Phys. Rev. B.* **1988**, *37*, 785–789.
(33) Toukan, K.; Rahman, A. *Phys. Rev. B.* **1985**, *31*, 2643–2648.
(34) Troullier, N.; Martins, J. L. *Phys. Rev. B.* **1991**, *43*, 1993–2006.
(35) Kleinman, L.; Bylander, D. M. *Phys. Rev. Lett.* **1982**, *48*, 1425.
(36) Goedecker, S.; Teter, M.; Hutter, J. *Phys. Rev. B.* **1996**, *54*, 1703–1710.
(37) Hartwigsen, C.; Goedecker, S.; Hutter, J. *Phys. Rev. B.* **1998**, *58*, 3641–3662.
(38) Nos′e, S. *J. Chem. Phys.* **1984**, *81*, 511.
(39) Nos′e, S. *Mol. Phys.* **1984**, *52*, 255.
(40) Hoover, W. G. *Phys. Rev. A.* **1985**, *31*, 1695.
(41) Kuo, I.-F. W.; Mundy, C. J.; McGrath, M. J.; Siepmann, J. I.; VandeVondele, J.; Sprik, M.; Hutter, J.; Chen, B.; Klein, M. L.; Mohamed, F.; Krack, M.; Parrinello, M. *J. Phys. Chem. B* **2004**, *108*, 12990–12998.
(42) Hetenyi, B.; Angelis, F. D.; Giannozzi, P.; Car, R. *J. Chem. Phys.* **2004**, *120*, 8632.
(43) Corcelli, S.; Skinner, J. L. *J. Phys. Chem. A* **2005**, *109*, 6154–6165.
(44) Smith, J. D.; Saykally, R. J.; Geissler, P. L. *J. Am. Chem. Soc.* **2007**, *129*, 13847.
(45) Woutersen, S.; Mu, Y.; Stock, G.; Hamm, P. *Chem. Phys.* **2001**, *266*, 137–147.
(46) Zheng, J.; Kwak, K.; Asbury, J. B.; Chen, X.; Piletic, I.; Fayer, M. D. *Science* **2005**, *309*, 1338–1343.
(47) Kim, Y. S.; Hochstrasser, R. M. *Proc. Natl. Acad. Sci. U.S.A.* **2005**, *102*, 11185–11190.
(48) Cahoon, J. F.; Sawyer, K. R.; Schlegel, J. P.; Harris, C. B. *Science* **2008**, *319*, 1820–1823.
(49) Steinel, T.; Asbury, J. B.; Zheng, J. R.; Fayer, M. D. *J. Phys. Chem. A* **2004**, *108*, 10957–10964.
(50) Dokter, A. M.; Woutersen, S.; Bakker, H. J. *Phys. Rev. Lett.* **2005**, *94*, 178301.
(51) Piletic, I.; Moilanen, D. E.; Spry, D. B.; Levinger, N. E.; Fayer, M. D. *J. Phys. Chem. A* **2006**, *110*, 4985–4999.
(52) Kropman, M. F.; Bakker, H. J. *J. Am. Chem. Soc.* **2004**, *126*, 9135–9141.
(53) Mukamel, S. *Principles of Nonlinear Optical Spectroscopy*; Oxford University Press: New York, 1995.
(54) Kwak, K.; Zheng, J.; Cang, H.; Fayer, M. D. *J. Phys. Chem. B.* **2006**, *110*, 19998–20013.
(55) Kwac, K.; Cho, M. *J. Chem. Phys.* **2004**, *120*, 1477–1490.
(56) Schmidt, J. R.; Corcelli, S. A.; Skinner, J. L. *J. Chem. Phys.* **2005**, *123* (13), 044513.
(57) Loparo, J. J.; Roberts, S. T.; Nicodemus, R. A.; Tokmakoff, A. *Chem. Phys.* **2007**, *341*, 218–229.
(58) Fecko, C. J.; Loparo, J. J.; Roberts, S. T.; Tokmakoff, A. *J. Chem. Phys.* **2005**, *122* (18), 054506.
(59) Kwak, K.; Park, S.; Finkelstein, I. J.; Fayer, M. D. *J. Chem. Phys.* **2007**, *127*, 1245031.
(60) Gordon, R. G. *J. Chem. Phys.* **1965**, *43*, 1307.
(61) Oxtoby, D. W. *Annu. Rev. Phys. Chem.* **1981**, *32*, 77.
(62) Silvestrelli, P. L.; Bernasconi, M.; Parrinello, M. *Chem. Phys. Lett.* **1997**, *277*, 478–482.
(63) Woods, K. N.; Wiedemann, H. *Chem. Phys. Lett.* **2004**, *393*, 159–165.
(64) Chandler, D. *Introduction to Modern Statistical Mechanics*; Oxford University Press, Inc: New York, 1987.
(65) Joo, T.; Jia, Y.; Yu, J. Y.; Lang, M. J.; Fleming, G. R. *J. Chem. Phys.* **1996**, *104*, 6089.
(66) Loparo, J. J.; Roberts, S. T.; Tokmakoff, A. *J. Chem. Phys.* **2006**, *125*, 194521.
(67) Flükiger, P.; Lüthi, H. P.; Portmann, S.; Weber, J. *MOLEKEL 4.0*; Swiss National Supercomputing Centre CSCS: Manno, Switzerland, 2000.

JP9016739